Spectroscopy 23 (2009) 81–101
DOI 10.3233/SPE-2009-0371
IOS Press

Short Review

Structural analysis of protein–DNA and protein–RNA interactions by FTIR, UV-visible and CD spectroscopic methods

H.A. Tajmir-Riahi *, C.N. N'soukpoé-Kossi and D. Joly
Department of Chemistry–Biology, University of Québec at Trois-Rivières, Trois-Rivières, QC, Canada

Abstract. In this chapter the fundamental question of how does protein–DNA or protein–RNA interaction affect the structures and dynamics of DNA, RNA and protein is addressed. Models for calf-thymus DNA and transfer RNA interactions with human serum albumin (HSA), ribonuclease A (RNase A) and deoxyribonuclease I (DNase I) are presented here, using Fourier Transform Infrared (FTIR) spectroscopy in conjunction with UV-visible and CD spectroscopic methods. In the models considered, the binding sites, stability and structural aspects of protein–DNA and protein–RNA are discussed and the effects of protein interaction on the secondary structures of DNA, RNA and protein were determined.

Keywords: DNA, protein, binding mode, binding constant, secondary structure, FTIR spectroscopy

Abbreviations

HSA: human serum albumin,
RNase A: ribonuclease A,
DNase I: deoxyribonuclease I,
G: guanine,
A: adenine,
T: thymine,
U: uracil,
FTIR: Fourier transform infrared,
CD: circular dichroism.

1. Introduction

Fourier Transform Infrared (FTIR) spectroscopy has widespread application to qualitative and quantitative analyses in chemistry, biochemistry, biology, medicinal chemistry and environmental science.

*Corresponding author: H.A. Tajmir-Riahi, Department of Chemistry–Biology, University of Québec at Trois-Rivières, C.P. 500, Trois-Rivières, QC, Canada G9A 5H7. Tel.: +1 819 376 5052 (ext. 3310); Fax: +1 819 376 5084; E-mail: tajmirri@uqtr.ca.

0712-4813/09/$17.00 © 2009 – IOS Press and the authors. All rights reserved

Its single most important use has been for the identification of organic compounds, drugs and pollutants. But now, FTIR spectroscopy is an established method for the structural characterization of proteins, DNA and RNA. For instance, FTIR spectroscopy with its secondary derivatives were used to determine protein conformation. Furthermore, changes in the secondary structure of proteins as a function of changes in pH, solvent composition, temperature, ligand binding, and exposure to DNA, RNA and lipids or other compounds in solution (e.g. drugs) have also been investigated. Similarly, DNA and RNA conformational transitions induced by ligand, drug or protein interactions were studied by FTIR spectroscopy. In addition, the application of FTIR in conjunction with Mass Spectrometry (MS), Ultra-Violet Spectrophotometer (UV), Nuclear Magnetic Resonance (NMR) and CD spectroscopy has been the most powerful method of identifying the chemical structures or subtle structural variations in biomacromolecules induced by ligand or drug interaction.

DNA–protein and RNA–protein interactions play important roles in a variety of biomolecular functions. Gene expression, transcription, replication, recombination, packaging and repairs all are controlled by DNA–protein interactions. Although the physical basis for these recognition processes is not fully understood, X-ray crystallography, NMR spectroscopy and molecular modeling provide us with a wealth of information on DNA recognitions [1–5]. The quantitative assessment of DNA–protein interaction is essential to understanding transcription, the beginning of biological processes including normal cellular function, development and many diseases [6]. RNA plays major role in diverse functions within the cell. Protein–RNA complexation is essential in many of these biological functions. Transfer RNAs bind to aminoacyl–tRNA synthetases for the translation of the genetic code during protein synthesis [7,8], while ribonucleoproteins bind RNA in post-transcriptional regulation of gene expression [9]. Although the biological significance of protein complexation with RNA has been well recognized, the specific mechanism of protein–RNA interaction is not fully understood [10]. Measurement of sequence–specific DNA–protein and RNA–protein interactions is a key experimental procedure in molecular biology of gene regulation. The most commonly used method is the electrophoretic gel mobility shift assay (EMSA), in which a radioactively labeled DNA probe is mixed with a solution of protein of interest and after a short reaction period, loaded on an electrophoretic gel [11]. Since there are some limitations using EMSA method, affinity capillary electrophoresis has been widely used to measure the mobility shift or zone electrophoresis to estimate the affinity of DNA–protein complexation [12–14].

Human serum albumin (Fig. 1(A)) is a principal extracellular protein with a high concentration in blood plasma (40 mg/ml) [15–18]. HSA is a globular protein composed of three structurally similar domains (I, II and III), each containing two sub-domains (A and B) and stabilized by 17 disulphide bridges [19–22]. Aromatic and heterocyclic ligands were found to bind within two hydrophobic pockets in sub-domains IIA and IIIA, namely site I and site II [19–22]. Seven binding sites are localized for fatty acids in sub-domains IB, IIIA, IIIB and on the sub-domains interfaces [16]. HSA has also a high affinity metal binding site at the N-terminus [15]. The multiple binding sites underlie the exceptional ability of HSA to interact with many organic and inorganic molecules and make this protein an important regulator of intercellular fluxes, as well as the pharmacokinetic behavior of many drugs [15–22].

RNase A (Fig. 1(B)) catalyzes the cleavage of P-O5′ bonds in RNA on the 3′ side of pyrimidine to form cyclic 2′,5′-phosphates under specific conditions [23–25]. Oligomers of RNase A exhibit antitumor activity [26]. In recent years, RNase A has been the molecular target for the development of small inhibitors. These inhibitors are developed to restrain biological activity of different RNase A homologs in a variety of pathological conditions [27–32].

DNase I (Fig. 1(C)) hydrolyses double stranded DNA predominantly by a single-stranded nicking mechanism under physiological conditions in the presence of Mg^{2+} and Ca^{2+} [33–35]. X-ray structural

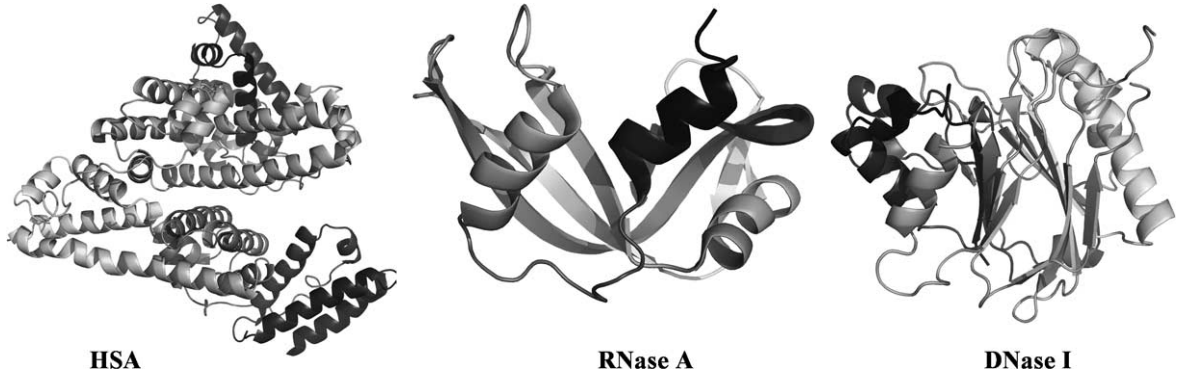

Fig. 1. Ribbon structure of human serum albumin (HSA) (A), RNase A (B), and DNase I (C) derived from their crystal structure determined by X-ray diffraction at 2.5 Å [17], 2.32 Å [58] and 2.8 Å [59], respectively.

analysis of DNase I–d(GCGATCGC)$_2$ and DNase I–d(GGTATACC)$_2$ complexes showed that protein binds to the minor groove and the backbone phosphate group with no contact with the major groove of the right-handed DNA duplexes, altering groove geometry as well as causing distortion of B–DNA conformation [36–39].

Structural analysis of calf-thymus DNA and transfer RNA interactions with HSA, RNase A and DNase I are presented here, using Fourier Transform Infrared (FTIR) in conjunction with UV-visible and CD spectroscopic methods. The binding sites, stability and structural aspects of protein–DNA and protein–RNA complexes are discussed and the effects of protein interaction on the secondary structures of polynucleotides and protein are reported here.

2. Experimental section

2.1. Materials

Highly polymerized type I calf-thymus DNA sodium salt (7% Na content) and Baker Yeast tRNA were purchased from Sigma Chemical Co., and deproteinated by the addition of $CHCl_3$ and isoamyl alcohol in NaCl solution. In order to check the protein content of DNA and RNA solutions, the absorbance at 260 and 280 nm was recorded. The A_{260}/A_{280} ratio was 1.85 for DNA and 2.1 for RNA showing that the polynucleotides were sufficiently free from protein. Human serum albumin (fatty acid free) fraction V and bovine pancreatic ribonuclease A (type XII-A) were from Sigma Chemical Company. Bovine pancreatic deoxyribonuclease I (type XII-A) was purchased from MP Biochemical Inc.

2.2. Preparation of protein–DNA and protein–RNA complexes

Sodium–DNA or sodium–tRNA was dissolved to 2% w/w (0.05 M DNA (phosphate)) in Tris-HCl buffer (pH 7.30 $\pm$ 0.1) at 5°C for 24 h with occasional stirring to ensure the formation of a homogeneous solution. The final concentration of the stock polynucleotide solution was determined spectrophotometrically at 260 nm by using molar extinction coefficient of 6600 cm^{-1} M^{-1} for DNA and 9250 cm^{-1} M^{-1}

for tRNA (expressed as molarity of phosphate group) [40,41]. The UV absorbance at 260 nm of a diluted solution (1/250) of calf-thymus DNA used in our experiments was measured to be 0.661 (path length was 1 cm) and the final concentration of the stock DNA solution was calculated to be 25 mM in DNA phosphate. The average length of the DNA molecules, estimated by gel electrophoresis was 9000 base pairs (molecular weight $\sim 6 \times 10^6$ Da). The appropriate amount of HSA was prepared in phosphate buffer (pH 7.3 ± 0.1). The protein solution then was added dropwise to DNA solution to attain desired protein concentration of 0.125 0.250, 0.500 and 1.000 mM with a final DNA or RNA concentration of 12.5 mM polynucleotide (phosphate) for infrared measurements. For capillary electrophoresis, mixtures contained various concentrations of HSA and constant concentration of DNA (2.5 mM phosphate) with protein–polynucleotide molar ratios of 1/250 to 1/55. The pH solution was adjusted to 6.80–7.30, using NaOH solution. The infrared spectra were recorded 1 h after incubation of protein with DNA or RNA solution.

2.3. FTIR spectra

For IR measurements, hydrated films containing various protein concentrations (34–300 μM) and constant nucleotide concentration of 12.5 mM were used. Infrared spectra were recorded on a Bomem DA3-0.02 FTIR spectrometer equipped with a nitrogen cooled HgCdTe detector and KBr beam splitter or on Nicolet FTIR spectrometer (Impact 420 model), equipped with DTGS (deuterated triglycine sulfate) detector and KBr beam splitter, using AgBr windows. The solution spectra are taken using AgBr windows with resolution of 2–4 cm^{-1} and 100–500 scans. The water subtraction was carried out with 0.1 M NaCl solution used as a reference at pH 6.5–7.5 [42]. A good water subtraction is achieved as shown by a flat baseline around 2200 cm^{-1}, where the water combination mode is located. This method is a rough estimate, but removes the water content in a satisfactory way [42]. The difference spectra [(polynucleotide solution + protein solution) − (polynucleotide solution)] are produced, using a sharp DNA band at 968 cm^{-1} and RNA band at 864 cm^{-1} as internal references. These bands, which are due to the sugar C–C and C–O stretching vibrations, exhibit no spectral changes (shifting or intensity variations) on protein–polynucleotide complexation and were cancelled upon spectral subtraction. The spectra are smoothed with a Savitzky–Golay procedure [25]. The intensity ratios of several DNA in-plane vibrations related to A–T and G–C and A–U base pairs and the PO_2 stretching are measured with respect to the reference band at 968 cm^{-1} or 864 cm^{-1} as a function of protein concentration with an error of ±3%. These intensity ratio measurements are used to quantify the amounts of protein binding to the backbone PO_2 group and DNA bases [43].

2.4. Analysis of protein secondary structure

Analysis of the secondary structure of DNase I and its tRNA complexes was carried out on the basis of the procedure reported [44]. The protein secondary structure is determined from the shape of the amide I band, located at 1650–1660 cm^{-1}. Fourier self-deconvolution and second derivative resolution enhancement were applied to increase the spectral resolution in the region of 1700–1600 cm^{-1}. The second derivatives were produced using a point convolution 11 or 13. The resolution enhancement resulting from self-deconvolution and the second derivative is such that the number and the position of the bands to be fitted are determined. In order to quantify the area of the different components of amide I contour, revealed by self-deconvolution and second derivative, a least-square iterative curve fitting was used to fit the Gaussian line shapes to the spectra between 1700–1600 cm^{-1}.

2.5. CD spectroscopy

CD spectra were recorded at pH 7.4 with a Jasco J-720 spectropolarimeter. For measurements in the Far-UV region (200–320 nm), a quartz cell with a path length of 0.01 cm was used. Three scans were accumulated at a scan speed of 50 nm per minute, with data being collected at every nm from 200 to 320 nm. Sample temperature was maintained at 25°C using a Neslab RTE-111 circulating water bath connected to the water-jacketed quartz cuvettes. Spectra were corrected for buffer signal and conversion to the Mol CD ($\Delta\varepsilon$) (for proteins) was performed with the Jasco Standard Analysis software. The protein concentrations used in our experiment were 0.35–35 μM, while tRNA and DNA concentration was fixed at 2.5 mM. The protein secondary structure was calculated using CONTINLL software [45] which predicts the different assignments of secondary structures by comparison with different ranges of proteins from high quality X-ray diffraction data [46]. The program CONTINLL is provided in CDPro software package which is available at the website: http://lamar.colostate.edu/∼sreeram/CDPro.

2.6. Absorption spectroscopy

The absorption spectra were recorded on a Perkin Elmer Lambda 40 Spectrophotometer. Quartz cuvettes of 1 cm were used. The absorbance measurements were performed at pH 7.4 by keeping the concentration of polynucleotide (40 μM) constant, while using different protein contents (1–20 μM).

The values of the binding constants K were obtained according to the methods reported [47,48]. By assuming that there is only one type of interaction between protein and polynucleotides in aqueous solution, the Eqs (1) and (2) can be established:

$$\text{Polynucleotide} + \text{protein} \Leftrightarrow (\text{polynucleotide} : \text{protein})\ \text{complex}, \tag{1}$$

$$K = [\text{polynucleotide} : \text{protein}]/[\text{polynucleotide}][\text{protein}]; \tag{2}$$

Polynucleotide = DNA or RNA and protein = HSA, RNase A or DNase I.

The values of the binding constants K were obtained from the DNA or RNA absorption at 260 nm according to the method described by published methods [47,48] where the bindings of various ligands to biomacromolecule were described. For weak binding affinities the data were treated using linear reciprocal plots based on:

$$\frac{1}{A - A_0} = \frac{1}{A_\infty - A_0} + \frac{1}{K(A_\infty - A_0)} \cdot \frac{1}{C_{\text{ligand}}}, \tag{3}$$

where, A_0 is the absorbance of DNA or RNA at 260 nm in the absence of protein, A_∞ is the final absorbance of the protein–polynucleotide complex and A is the recorded absorbance of complexes at different protein concentrations. Thus, the double reciprocal plot of $1/(A - A_0)$ vs. $1/C_{\text{protein}}$ is linear and the binding constant (K) can be estimated from the ratio of the intercept to the slope [47,48].

3. Results and discussion

3.1. FTIR spectra of HSA–DNA and HSA–RNA adducts

In order to characterize the protein–DNA bindings the infrared spectra of HSA–DNA complexes were recorded using constant amount of DNA with various concentrations of protein and the results are pre-

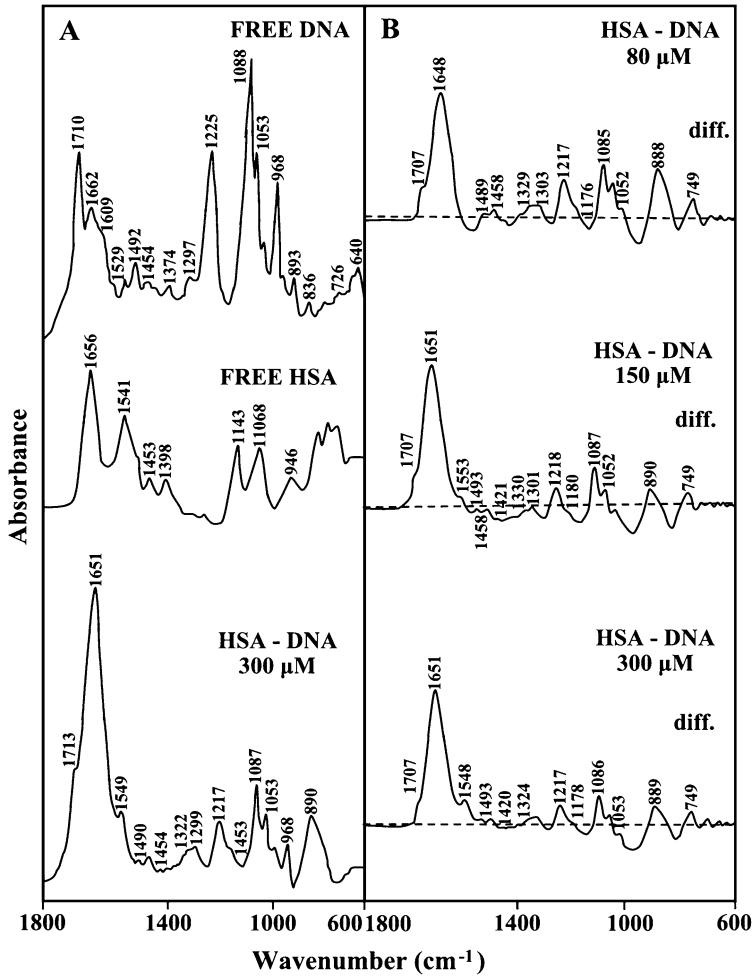

Fig. 2. FTIR spectra (A) and difference spectra [(DNA solution + protein solution) − (DNA solution)] (B) in the region of 1800–1500 cm^{-1} for the free DNA and human serum albumin (HSA) and their complexes in aqueous solution at physiological pH with various protein concentrations.

sented in Fig. 2(A) and (B). The DNA in-plane vibrations at 1750–1500 cm^{-1} related to the G–C and A–T base pairs and the back bone phosphate group at 1250–1000 cm^{-1} [42,43,49–52] were perturbed upon protein interaction. The mainly guanine carbonyl vibration at 1710 cm^{-1} of the free DNA gained intensity and shifted towards a higher frequency at 1713 cm^{-1} upon HSA complexation (Fig. 2(A)). Similarly, an increase in the intensity of the backbone PO_2 asymmetric stretching band at 1225 cm^{-1} was observed, which shifted towards a lower frequency at 1210 cm^{-1}, in the spectra of HSA–DNA complexes (Fig. 2(A)). The positive features at 1707 and 1217–1218 cm^{-1} in the difference spectra of HSA–DNA complexes are coming from an increase in the intensity of the guanine band at 1710 and the PO_2 band at 1225 cm^{-1}, respectively (Fig. 2(B)). In addition to a major spectral shifting of the PO_2 stretching at 1225 cm^{-1}, the relative intensities of the asymmetric (ν_{as}) and symmetric (ν_s) stretching vibrations of the backbone phosphate group were altered upon HSA interaction [42]. The ν_s PO_2 (1088 cm^{-1}) and ν_{as} PO_2 (1225 cm^{-1}) have changed, with the ratio ν_s/ν_{as} going from 1.75 (free DNA) to 1.55 (protein–DNA complexes). The observed spectral changes are due to the participation

of the G–C bases (mainly guanine) and the backbone PO_2 group in the HSA–DNA interactions. Similar alterations of the phosphate group vibrational frequencies were observed in the infrared spectra of the calf-thymus DNA–polypeptide complexes, where the protein–nucleic acid interaction was mainly through the backbone phosphate group and the positively charged amino acids on the surface of protein [53,54]. Therefore, it can be assumed that the protein bindings are mainly through G–C bases and the backbone phosphate groups in the HSA–DNA adducts.

No major protein–RNA interaction occurs with HSA at low concentration (40 μM). Evidence for this comes from lack of spectral changes for several RNA in-plane vibrations at 1698 (mainly guanine), 1654 (mainly uracil), 1608 (adenine), 1488 (mainly cytosine) and 1244 cm^{-1} (asymmetric PO_2 stretch) [42,49–52] upon HSA interaction. As protein concentration increased to 80 μM, minor intensity increases were observed for the PO_2 bands at 1244 and 1087 cm^{-1}, with positive features at 1244 and 1088 cm^{-1} in the difference spectra of protein–RNA complexes (Fig. 3(A) and (B)). The observed spectral changes are indicative of some degree of protein–PO_2 interaction. As HSA content increased to

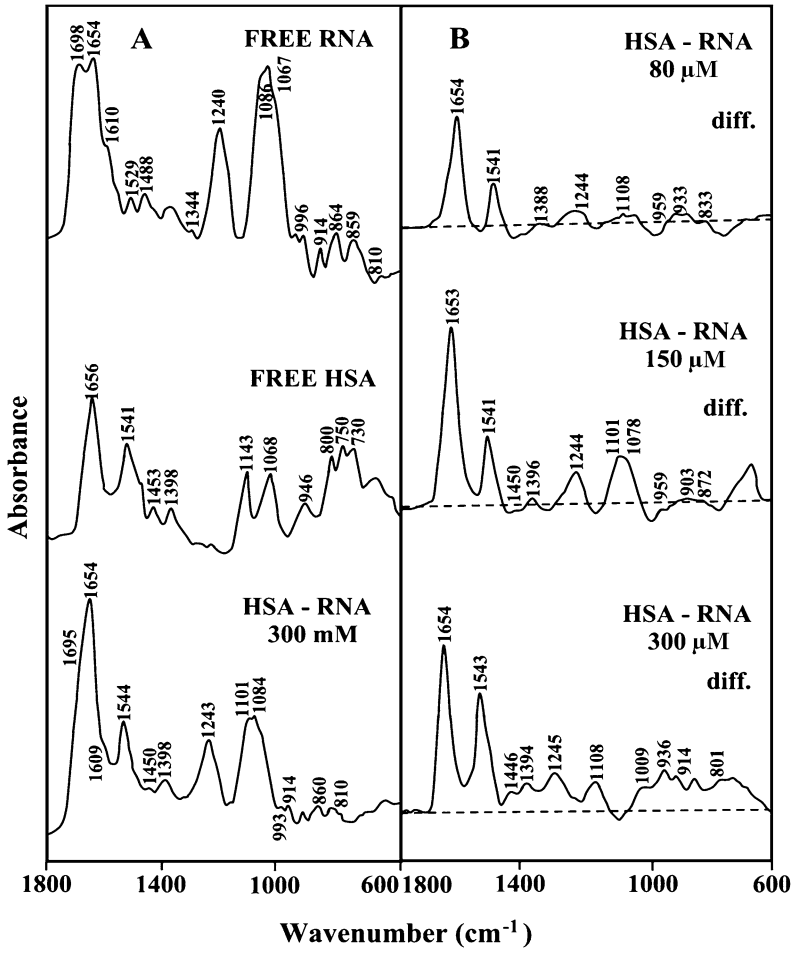

Fig. 3. FTIR spectra (A) and difference spectra [(tRNA solution + protein solution) − (tRNA solution)] (B) in the region of 1800–1500 cm^{-1} for the free tRNA and human serum albumin (HSA) and their complexes in aqueous solution at physiological pH with various protein concentrations.

300 μM, the guanine band at 1698 cm^{-1} shifted to a lower frequency at 1695 cm^{-1} in the spectra of protein–RNA adducts (Fig. 3(A)). The shifting of the guanine band at 1698 cm^{-1} was also accompanied by major intensity variations of this band upon HSA interaction. The changes observed are due to protein interaction with guanine bases in HSA–RNA complexes. Further evidence regarding HSA–PO_2 interaction is also coming from the intensity ratio alterations of symmetric and asymmetric PO_2 bands at 1086/1240 cm^{-1} [42]. The ratio of ν_s/ν_{as} was changed from 1.55 (free RNA) to 1.40 (complexed RNA) upon HSA interaction (Fig. 3(A), 300 μM). It has been suggested that many proteins bind DNA or RNA through positively charged amino acids on their surfaces [54]. Such positive charge can bind the negatively charged backbone PO_2 group through electrostatic interactions.

Additional evidence regarding HSA–DNA and HSA–RNA interactions comes from a major shifting of the protein amide I at 1656 and amide II band at 1541 cm^{-1} [55]. The amide I band at 1656 cm^{-1} shifted towards lower frequencies at 1651 (HSA–DNA), whereas the amide II band at 1541 cm^{-1} shifted towards higher frequencies at 1549 (HSA–DNA) upon DNA–protein interaction (Figs 2(A) and 3(A)). Similarly, the protein amide A band at 3300 cm^{-1} (NH stretching) [37] shifted towards a lower frequency at 3290 cm^{-1} upon HSA–DNA and HSA–RNA adduct formation (spectra not shown). The observed spectral changes are indicative of protein–polynucleotide interaction *via* polypeptide C=O, C–N and NH groups (H-bonding).

3.2. HSA conformation

DNA and RNA interactions with HSA induced no major alterations of the protein secondary structure. Conformational analysis of the free HSA in H_2O solution shows α-helix 55% (1656 cm^{-1}), β-sheet 22% (1616–1635 cm^{-1}), β-anti 12% (1684 cm^{-1}) and 11% turn 11% (1673 cm^{-1}) (Fig. 4(A) and Table 1) [56]. The random structure was estimated 12% from D_2O solution (1640–1645 cm^{-1}). The second derivative and curve-fitting procedures [37,38] were applied to the protein amide I band (at 1651 cm^{-1} of the difference spectra of HSA–DNA and RNA adducts). The results showed no major alterations of the HSA secondary structure, on DNA and RNA complexation (Figs 4(B) and 3(C) and Table 1). This is indicative of some degree of stabilization of the protein secondary structure upon polynucleotide interaction.

3.3. FTIR spectra of RNase–DNA and RNase–RNA adducts

The IR spectral features of RNase–DNA interaction are presented in Fig. 5. Evidence for protein–DNA binding comes from spectral changes observed for both free DNA and free RNase upon complexation. The band at 1710 cm^{-1} of the free DNA spectrum assigned mainly to guanine bases [42,43,49–52] gained intensity in the spectra of RNase–DNA complexes (Fig. 5). The increase in intensity is clearly shown in difference spectra of RNase–DNA complexes (Fig. 5, diff., 34 and 270 μM). The presence of positive features at 1709 (DNA), 1660 (protein) and 1646 cm^{-1} (protein), in the difference spectra are due to increase in intensities of DNA and RNase vibrations. The positive peak at 1709 cm^{-1} is due to increase in intensity of DNA band at 1710 cm^{-1} (guanine), while the positive bands at 1660 and 1646 cm^{-1} are due to RNase amide I band at 1659 and 1644 cm^{-1} (Fig. 5, diff., 34 and 270 μM). The spectral changes observed are due to the participation of DNA bases (G) in the RNase complexation. The protein–PO_2 interaction is also evident from increase in intensity and shifting of the PO_2 asymmetric band at 1225 cm^{-1}, which appeared at 1228 cm^{-1} in the spectra of the RNase–DNA complexes (Fig. 5, 270 μM). The positive features at 1212 and 1218 cm^{-1} (Fig. 5, diff. 34 and 270 μM) are due to increase

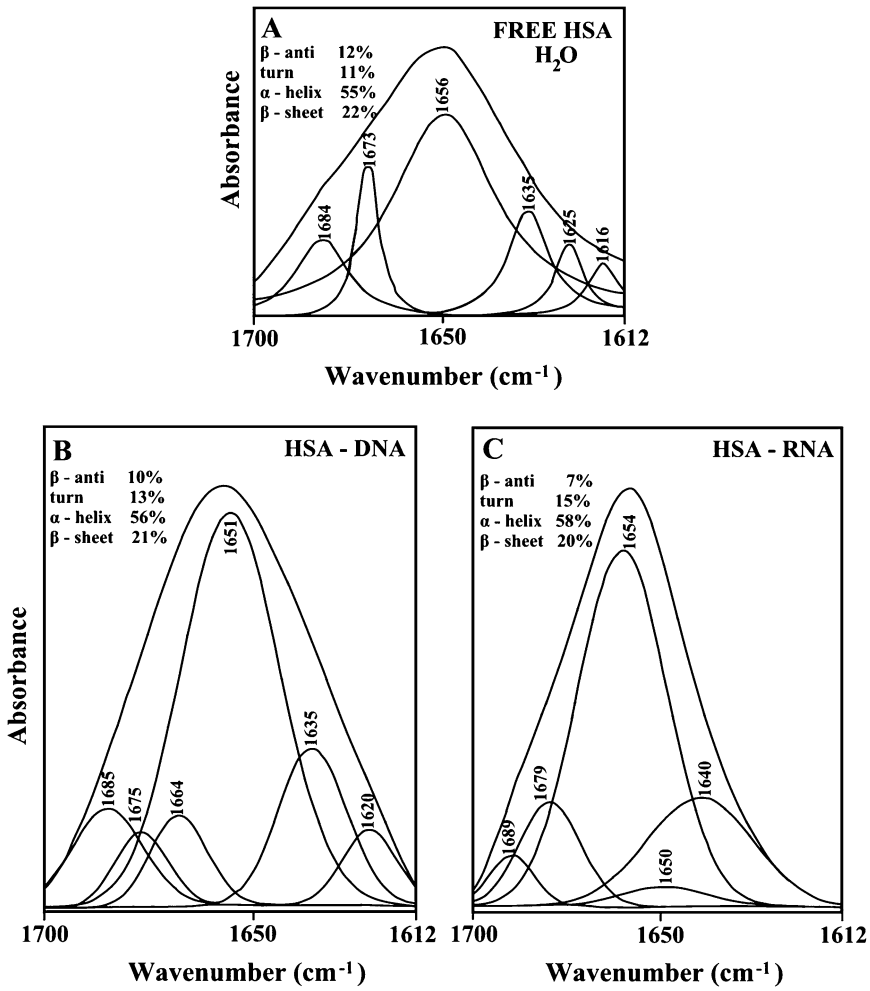

Fig. 4. Curve-fitted amide I region (1700–1612 cm^{-1}) and secondary structure determination of the free human serum albumin (A) and its HSA–DNA (B), and HSA–tRNA (C) in aqueous solution with 300 μM protein and 12.5 mM polynucleotide concentrations.

in intensity of the asymmetric PO_2 band at 1225 cm^{-1} upon protein interaction (Fig. 5, diff. 34 and 270 μM). Further evidence regarding RNase–PO_2 interaction is also coming from the intensity ratio variations of symmetric and asymmetric PO_2 bands at 1086/1225 [42]. The ratio of ν_s/ν_{as} was changed from 1.50 (free DNA) to 1.80 (complexed DNA) upon RNase interaction (Fig. 5, 270 μM).

Evidence for RNase–tRNA interaction comes from infrared spectral analysis of both tRNA and RNase A presented in Fig. 6. The band at 1698 cm^{-1} of tRNA spectrum assigned mainly to guanine bases [42,43,49–52] gained intensity and shifted towards a lower frequency at 1689 cm^{-1} upon RNase interaction (Fig. 6). The increase in intensity and shifting are clearly observed in difference spectra of RNase–tRNA complexes with protein concentrations of 34 and 270 μM (Fig. 6, diff.). The presence of positive features at 1691 cm^{-1} (RNA), 1661 cm^{-1} (RNA), and 1643 and 1545 cm^{-1} (RNase) in the difference spectra are coming from both tRNA and RNase due to increase in intensities of these vibrations in the complexes. The positive peak at 1691 cm^{-1} is due to increase in intensity of tRNA band at

Table 1
Secondary structure analysis of the free HSA, RNase A, and DNase I and their DNA and RNA complexes in H_2O at physiological pH at 25°C

Amide I components (cm^{-1})	Free HAS H_2O (%)	HSA–DNA	HSA–RNA	Free RNase H_2O (%)	RNase–DNA	RNase–RNA	Free DNase H_2O (%)	DNase–DNA	DNase–RNA
1692–1680 β-anti	12.0 ± 1	12.0	7.0	9.0	12.0	4.0	2.0	7.0	8.0
1680–1660 turn	11.0 ± 1	13.0	15.0	16.0	12.0	31.0	12.0	110	15.0
1660–1649 α-helix	55.0 ± 3	56.0	58.0	28.0	16.0	18.0	40.0	27.0	27.0
1648–1641 random	11 ± 1.0	–	–	9.0	17.0	17.0	12	20.0	15.0
1640–1615 β-sheet	22.0 ± 2	21.0	20.0	38.0	43.0	30.0	34.0	35.0	34.0

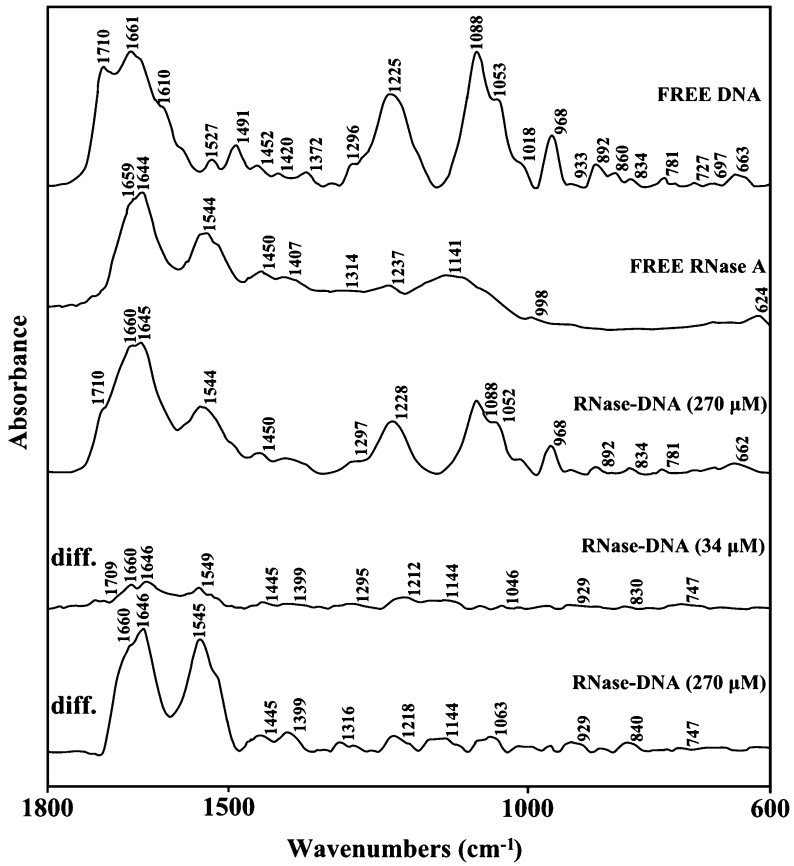

Fig. 5. FTIR spectra and difference spectra [(DNA solution + RNase A solution) − (DNA solution)] in the region of 1800–600 cm^{-1} for the free calf-thymus DNA (12.5 mM) and free RNase (270 μM) and their complexes in aqueous solution at pH 7.3 with various protein concentrations (34 and 270 μM) and constant DNA concentration (12.5 mM).

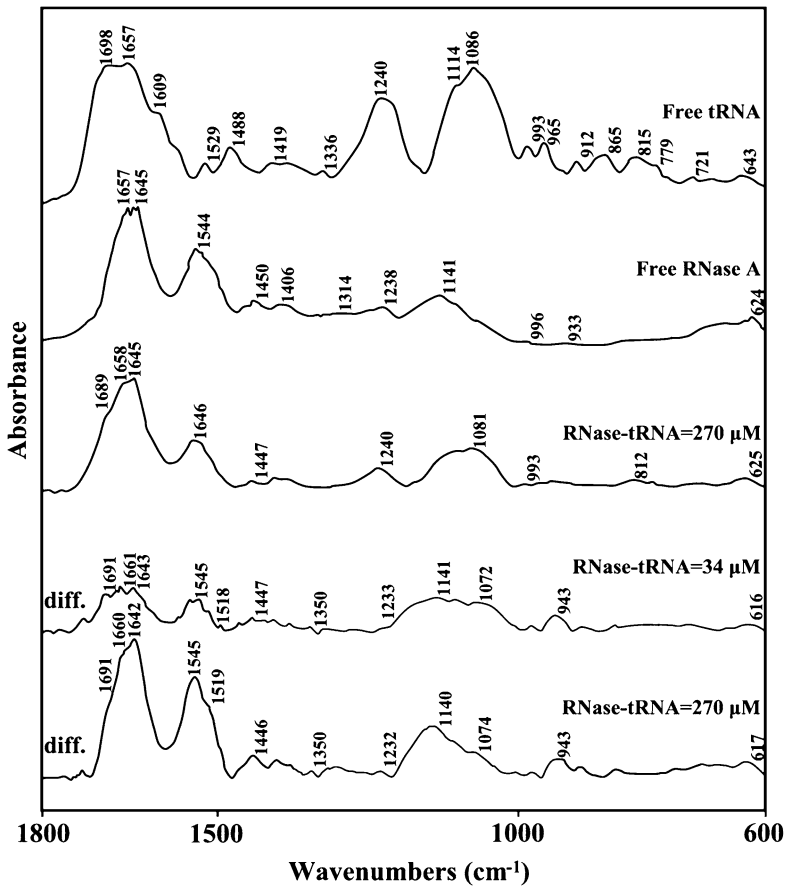

Fig. 6. FTIR spectra and difference spectra [(tRNA solution + RNase A solution) − (tRNA solution)] in the region of 1800–600 cm^{-1} for the free tRNA (12.5 mM) and free RNase (270 μM) and their complexes in aqueous solution at physiological pH (7.4) with various protein concentrations (34–270 μM).

1698 cm^{-1} (guanine), while the positive band at 1661 cm^{-1} can arise from uracil band at 1657 cm^{-1} and RNase amide I band at 1657 cm^{-1} (Fig. 6, diff., 34 μM). Because amide I band at 1657 cm^{-1} did not exhibit major shifting upon RNA complexation (the feature at 1661 should result from the uracil vibration at 1657 cm^{-1}) (Fig. 6, diff., 34 μM)), the spectral changes observed are due to the participation of RNA bases (G and U) in RNase complexation. Major protein–PO_2 interaction is also evident from the remarkable reduction in intensity of the PO_2 asymmetric band at 1240 cm^{-1} and increase in intensity of symmetric stretching at 1086 cm^{-1} with a characteristic positive feature at 1072 cm^{-1} (Fig. 6, diff., 34 μM). Further evidence regarding RNase–PO_2 interaction also comes from the intensity ratio variations of symmetric and asymmetric PO_2 bands at 1086/1240 (Alex and Dupuis, 1989). The ratio of ν_s/ν_{as} was changed from 1.30 (free RNA) to 1.90 (complexed RNA) upon RNase interaction (Fig. 6, 270 μM).

At high protein concentration (270 μM), the guanine band showed increase in intensity and appeared at 1691 cm^{-1} in the difference spectra (Fig. 6, diff., 270 μM), while protein amide I and amide II were shifted at 1660, 1642 and 1545 cm^{-1}. These spectral changes are the result of continued interaction of protein with RNA at high RNase content. The presence of positive features at 1232 and 1074 cm^{-1} in

the difference spectra come from the spectral changes of asymmetric and symmetric PO_2 vibrations due to a major protein–phosphate interaction (Fig. 6, diff., 270 μM).

3.4. RNase A conformation

The results of conformational analysis (IR spectroscopy) of the free RNase A and its DNA and RNA adduct is shown in Fig. 7 and Table 1). The free RNase A in H_2O solution shows α-helix 28% (1658 cm^{-1}), β-sheet 38% (1618–1638 cm^{-1}), β-anti 9% (1692 cm^{-1}), turn 16% (1679 cm^{-1}) and random coil 9% (1648 cm^{-1}) (Fig. 7(A)) consistent with crystal structure of RNase A, which contains mainly β-sheet structure [58]. No major alterations of protein conformation were observed upon DNA interaction at low RNase concentration (34 μM). However, at high protein content (270 μM), major reduction of α-helix from 28 to 16% and increase of β-sheet from 38 to 43% and random coil from 9 to 17% were observed (Fig. 7(B) and Table 1).

The results of conformational analysis RNase–tRNA complexes are shown in Fig. 7(C). No major alterations of protein conformation were observed upon RNA interaction at low RNase concentration (3.5 μM). However, at high protein content (270 μM), a major reduction of α-helix from 28 to 18% and

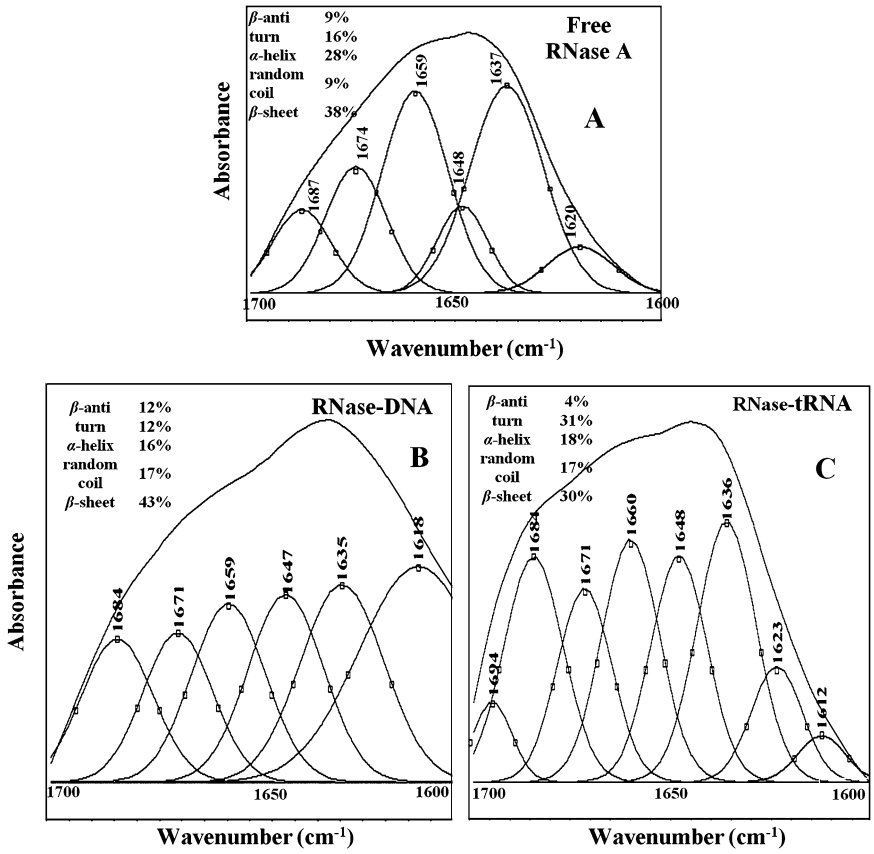

Fig. 7. Curve-fitted amide I region (1700–1600 cm^{-1}) obtained from IR spectra with secondary structure determination of the free RNase A (A) and its DNA (B) and tRNA (C) complexes in aqueous solution with 270 μM protein concentration and final polynucleotide content 12.5 mM at pH 7.4.

of β-sheet from 38 to 30% was observed (Fig. 7(C) and Table 1). The reduction in α-helix (from 28 to 18%) and β-sheet (from 38 to 30%) structure was associated with increase in turn structure from 16 to 31% and in random coil structure from 9 to 17% in the protein–tRNA complexes (Fig. 7(C), Table 1). The reduction of α-helix and β-sheet structure in favor of random coil can be attributed to a partial unfolding of protein upon tRNA complexation. The reduction of α-helix was also observed during heat denaturation of RNase A shown by infrared spectroscopy [57].

3.5. FTIR spectra of DNase–DNA and DNase–RNA adducts

The IR spectral features of DNase–DNA interaction are presented in Fig. 8. Evidence for protein–DNA binding comes from spectral changes observed when comparing both free DNA and free DNase spectra and their complexes. To begin, the band located at 1710 cm^{-1} of the free DNA spectrum assigned mainly

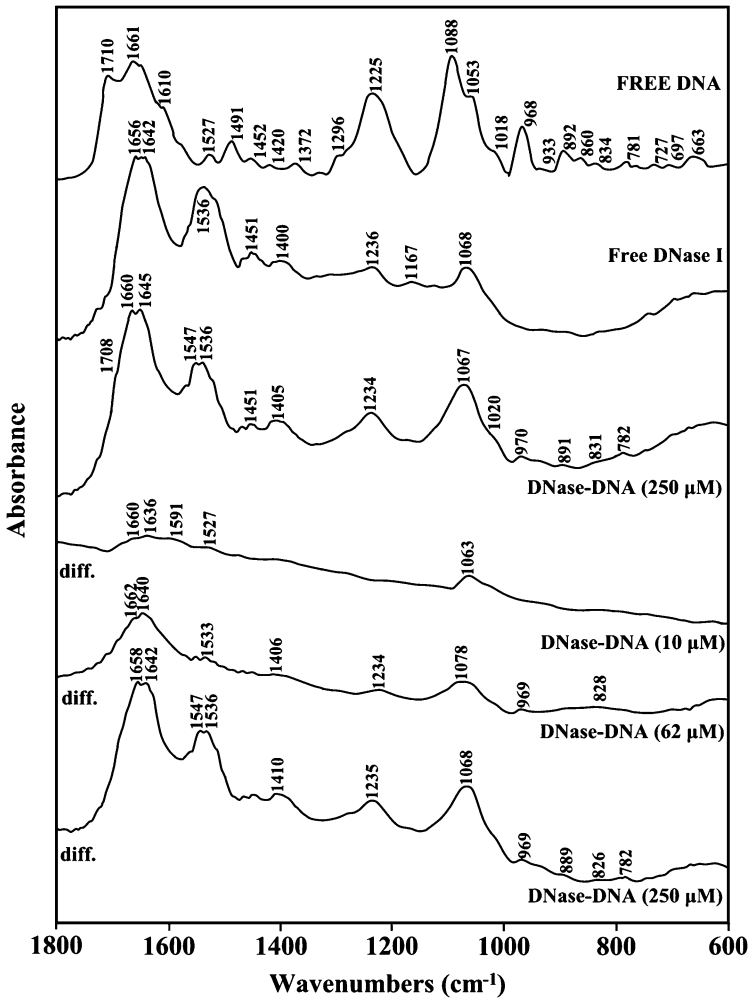

Fig. 8. FTIR spectra and difference spectra [(DNA solution + DNase I solution) − (DNA solution)] in the region of 1800–600 cm^{-1} for the free calf-thymus DNA (12.5 mM) and free DNase (250 μM) and their complexes in aqueous solution at pH 7.4 with various protein concentrations (10, 62 and 250 μM) and constant DNA concentration (12.5 mM).

to guanine bases [42,43,49–52] exhibited no major intensity variations in the spectra of DNase–DNA complexes (Fig. 8). But, the thymine band at 1661 cm^{-1} showed major intensity increase with a positive peak at 1660 in the difference spectra, upon DNase interaction (Fig. 8, diffs, 10 and 62 μM). Similarly the adenine band at 1610 cm^{-1} of the free DNA spectrum gained intensity with a positive feature at 1591 cm^{-1}, in the difference spectra of protein–DNA complexes (Fig. 8, diff., 10 μM). Since thymine band at 1660 cm^{-1} and protein amide I band at 1656 cm^{-1} are overlapped at high protein concentration, it is difficult to attribute the presence of the strong positive feature found at 1658 cm^{-1} to thymine or protein vibrations separately (Fig. 8, diff., 250 μM). The overall spectral changes observed for the thymine and adenine bands are due to major interaction of protein with A–T bases in the minor groove of DNA duplex. However, the other protein binding site is located at the backbone phosphate group. The major shifting of the PO_2 asymmetric vibration at 1225–1234 cm^{-1} and the symmetric vibration at 1088–1067 cm^{-1} is due to protein–PO_2 interaction (Fig. 8).

Additional DNase–DNA interaction is evidenced by shifting of the protein amide I band at 1642–1645 cm^{-1}, upon protein–DNA complexation. Similarly, the protein amide II band at 1536 cm^{-1} appeared with a new component band at 1545 cm^{-1} in the spectrum of protein–DNA complexes (Fig. 8, 250 μM). The observed spectral changes for amide I and amide II bands are due to protein–DNA interaction *via* polypeptide C=O, C–N and N–H groups (H-bonding).

Results presented in Fig. 9 and the analysis of infrared spectra of both tRNA and DNase I showed major DNase I–tRNA interaction. The band at 1698 cm^{-1} of tRNA spectrum assigned mainly to guanine bases [42,43,49–51] gained intensity and shifted towards a lower frequency at 1690 cm^{-1} upon DNase I interaction (Fig. 9). The increase in intensity and shifting is clearly evident in difference spectra of DNase I–tRNA complexes with protein concentrations of 10 μM (Fig. 9, diff. 10 μM). Indeed, positive features at 1681 and 1648 cm^{-1} in the difference spectra which come from tRNA are the result of increase in intensities of guanine band at 1698 and uracil band at 1660 cm^{-1} (Fig. 9, diff., 10 μM). However, the positive peaks at 1648 and 1536 cm^{-1} in the difference spectra with 10 and 62 μM protein concentration come from protein amide I and amide II vibrations (Fig. 9, diff., 10 and 62 μM). The spectral changes observed for the guanine band at 1690 and uracil band at 1660 cm^{-1} arise from the participation of RNA bases (G and U) in protein complexation. Major protein–PO_2 interaction is also evident from the increase in intensity and the shifting of the backbone PO_2 asymmetric band at 1240 cm^{-1} and symmetric stretching at 1085 cm^{-1} (Fig. 9, 250 μM). Further evidence regarding protein–PO_2 interaction is also coming from the intensity ratio variations of symmetric and asymmetric PO_2 bands at 1085/1240 (Alex and Dupuis, 1989). The ratio of ν_s/ν_{as} was changed from 1.65 (free tRNA) to 2 (complexed RNA) upon DNase interaction (Fig. 9, 250 μM).

At high protein concentration (250 μM), due to overlapping of tRNA in-plane vibrations with protein amide I vibrations in the region of 1659–1650 cm^{-1}, it is difficult to draw a firm conclusion about the nature of the protein–tRNA binding (Fig. 9, 250 μM). However, additional evidence regarding DNase I–tRNA interaction comes from shifting of the protein amide I bands at 1656, 1642 cm^{-1} and amide II band at 1536 cm^{-1}. The amide I band at 1656 cm^{-1} shifted towards a higher frequency at 1657 and the band at 1645 observed at 1638 cm^{-1}, while amide II band at 1536 shifted towards a higher frequency at 1542 cm^{-1} upon protein–tRNA complexation (Fig. 9, 250 μM). In the difference spectra of DNase I–tRNA, the bands at 1655 and 1638 cm^{-1} are coming from protein amide I bands, while the band at 1542 cm^{-1} is related to amide II bands (Fig. 9, diff., 250 μM). The observed spectral changes for amide I and amide II bands are indicative of protein–tRNA interaction *via* polypeptide C=O, C–N and NH groups (H-bonding).

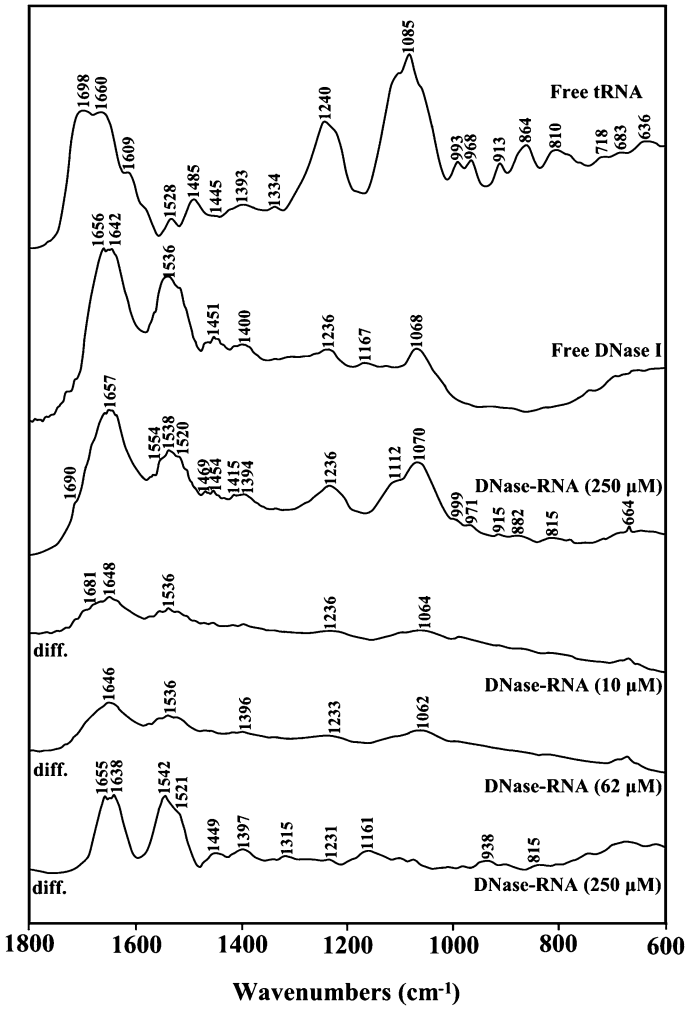

Fig. 9. FTIR spectra and difference spectra [(tRNA solution + DNase I solution) − (tRNA solution)] in the region of 1800–600 cm^{-1} for the free RNA (12.5 mM) and free DNase (250 µM) and their complexes in aqueous solution at pH 7.4 with various protein concentrations (10, 62 and 250 µM) and constant tRNA concentration (12.5 mM).

3.6. DNase I conformation

The results of conformational analysis (IR spectroscopy) of the free DNase I and its DNA complex are shown in Fig. 10(A). The free DNase I in buffer solution shows extensive α-helix 40% (1659 cm^{-1}), central β-sheet 34% (1612–1630 cm^{-1}), β-anti 2% (1692 cm^{-1}), turn 12% (1680 cm^{-1}) and random coil 12% (1642 cm^{-1}) (Fig. 10(A) and Table 1) that are consistent with structural analysis of DNase I [59]. At high protein content (250 µM), major reduction of α-helix from 40 to 27% and increase of random coil from 12 to 20% and β-anti from 2 to 7% were observed (Fig. 10(B) and Table 1). The reduction of α-helix and increase in β-anti and random coil structures are attributed to a partial unfolding of protein upon DNA complexation. These results are consistent with the reduction of α-helix observed during protein unfolding in protein polyamine complexes [56].

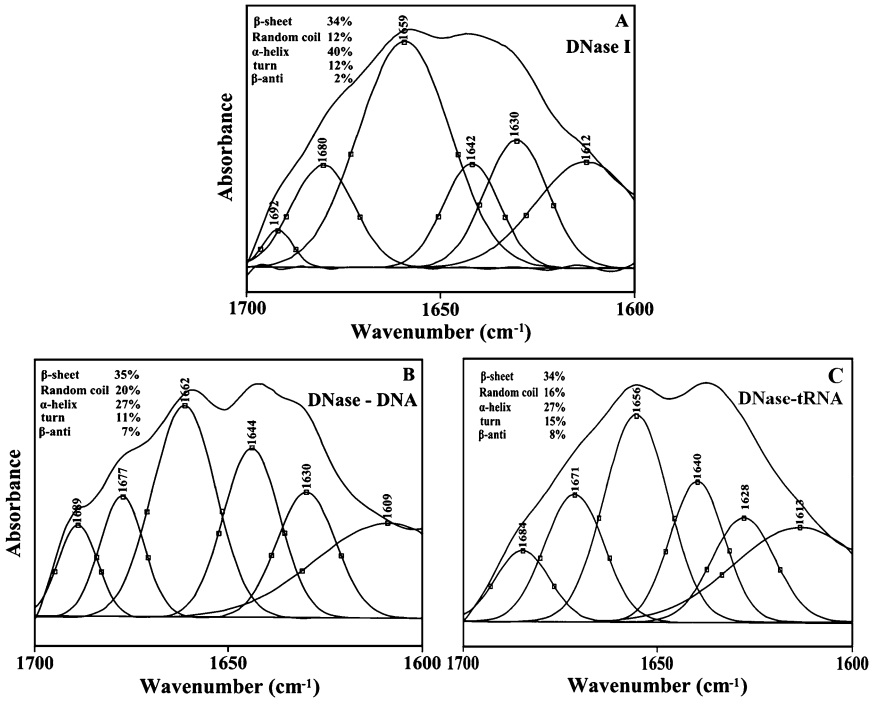

Fig. 10. Curve-fitted amide I region (1700–1600 cm^{-1}) with secondary structure determination of the free DNase I (A) and its DNA (B) and tRNA (C) complexes in aqueous solution with 250 μM protein concentration and final polynucleotide content 12.5 mM at pH 7.4.

The conformational changes of DNase I–tRNA complexes are shown in Fig. 10(C). The free DNase I in buffer solution shows extensive α-helix 40% (1659 cm^{-1}), central β-sheet 34% (1612–1630 cm^{-1}), β-anti 2% (1692 cm^{-1}), turn 12% (1680 cm^{-1}) and random coil 12% (1642 cm^{-1}) (Fig. 10(A)) that are consistent with structural analysis of DNase I [59]. At high protein content (250 μM), major reduction of α-helix from 40 to 27% and increase of random coil from 12 to 16%, β-anti from 2 to 8% and turn from 12 to 15% were observed (Fig. 10(C) and Table 1). The central β-sheet remained unchanged. The reduction of α-helix and increase in β-anti and random coil structures are attributed to a partial unfolding of protein upon tRNA complexation.

3.7. DNA and RNA conformations

Minor alterations of B–DNA structure were observed upon HSA complexation. Evidence for this comes from the spectral change for B–DNA marker bands at 1222 cm^{-1} (PO_2 stretch) and 1717 cm^{-1} (mainly guanine) [49,50,60], upon protein complexation (Fig. 2(A)). Other B–DNA indicator at 836 cm^{-1} (phosphodiester mode), was overlapped by the several protein bands centered at about 800 cm^{-1} (Fig. 2(A)). In a B to A transition, the marker band at 837 cm^{-1} shifts towards a lower frequency at about 810 cm^{-1} and the guanine band at 1717 cm^{-1} appears at 1700 cm^{-1}, while the phosphate band at 1222 cm^{-1} shifts towards a higher frequency at 1240 cm^{-1} [50,60]. In a B to Z conformational changes, the sugar–phosphate band at 836 cm^{-1} appears at 800–780 cm^{-1}, and the guanine band displaces to 1690 cm^{-1}, while the phosphate band shift to 1216 cm^{-1} [50,60]. The shifting of the bands at 1717 (G) to 1713 and 1222 (PO_2 stretch) to 1217 cm^{-1} are due to some degree of

DNA conformational changes upon protein interaction. The changes are due to minor perturbations of B–DNA structure towards Z-conformation. However, it is not a complete Z-formation, while the band at 1717 cm^{-1} appeared at 1713 cm^{-1} (in a complete Z structure this band appeared at 1690 cm^{-1}), while the shift of the PO_2 band at 1222–1217 cm^{-1} is consistent with Z-conformation (Fig. 2(A)). However, no conformational changes occurred for tRNA upon HSA adduct formation. Evidence for this is given by the absence of major alterations of A–RNA marker bands at 1698–1695 cm^{-1} (guanine), 1244–1243 cm^{-1} (phosphate) and 810 cm^{-1} (ribose–phosphate) (Fig. 3(A)) in both free tRNA and its protein complexes [61,62].

The DNase I–DNA interaction induced a partial DNA conformational transition. The CD spectrum of the free DNA is composed of four major peaks at 214 (negative), 225 (positive), 245 (negative) and 280 nm (positive) (not shown). This is consistent with the CD spectrum of double helical DNA in B conformation [63–65]. Upon addition of DNase I (25 and 62 μM), major shifting of CD bands were observed (spectra not shown). The band at 214 nm shifted to 208–210 nm and the one at 280 appeared at 271 nm upon protein complexation [65]. In a complete B to A transition, the CD marker bands at 214 nm lost intensity, the positive band at 225 nm shifted towards higher wavelength, while the positive band at 280 nm gained intensity and shifted to 267 nm [63]. The spectral changes reported for A–DNA were consistent with the double helical RNA in A conformation [64]. Since the major band at 280 nm shifted to 271 nm, the alterations of DNA structure is consistent with a partial B to A transition upon DNase interaction [66]. This is consistent with the infrared results on the DNase–DNA complexes that showed a partial B to A–DNA transition with shifting of the marker B-DNA bands at 1710 cm^{-1} (G) to 1708 cm^{-1}, 1225 cm^{-1} (PO_2) to 1234 cm^{-1}, and 834 cm^{-1} (phosphodiester modes) to 831 cm^{-1} (Fig. 8). In a complete B to A transition, the B–DNA marker IR bands are observed at 1700 cm^{-1} (G), 1240 cm^{-1} (PO_2) and 810 cm^{-1} (phosphodiester) [49,50,60]. However, the major intensity increase of the bands at 214 and 280 nm in the CD spectra of protein–DNA complexes are attributed to the base destacking interaction upon DNase complexation.

The CD spectrum of free tRNA is composed of three major peaks at 207 (negative), 220 and 269 nm (positive) (not shown). This is consistent with the CD spectrum of double helical RNA in A conformation [63–65]. Upon addition of DNase I (25.0 μM), no major shifting of the bands were observed, while an increase of the molar ellipticity of the band at 207 nm was observed [67]. However, as protein concentration increased (62.5 μM), major increase in molar ellipticity of the band at 207 nm and minor increase in intensity of the band at 269 nm were observed [67]. Since there was no major shifting of the bands at 207 and 269 nm, tRNA remains in A-conformation. However, the major alterations of the intensity of the band at 207 nm can be attributed to the reduction of the base stacking interaction and tRNA aggregation upon protein complexation. This is consistent with the infrared data on the DNase I–tRNA adducts that showed tRNA in A-conformation with marker IR bands at 1698 (G), 1240 (PO_2) and 865 and 815 cm^{-1} (phosphodiester modes) [49,50] in both free tRNA and in DNase I–RNA complexes (Fig. 9). It is important to note that there has been no digestion of tRNA by DNase I because no major structural changes occurred for tRNA under our experimental conditions (Fig. 9, infrared spectra).

RNase–DNA complexation did not alter DNA conformation. Evidence for this comes from no major alterations of the IR and CD marker bands of B–DNA upon RNase interaction. The CD spectrum of the free B–DNA is composed of four major peaks at 214 (negative), 225 (positive), 245 (negative) and 280 nm (positive) exhibit no major changes upon RNase A complexation. Similarly, the IR marker bands for B–DNA at 1710, 1225, 834 cm^{-1} showed no major alterations in the spectra of RNase–DNA complexes (Fig. 5). These are consistent with DNA remaining in B-family structure upon RNase

interaction. Similarly, the CD spectrum of free tRNA, which is composed of three major peaks at 207 (negative), 220 and 269 nm (positive) and the IR marker bands at 1698, 1240, 865 and 810 cm^{-1} (Fig. 6) showed no major spectral changes on RNase complexation. This is indicative of tRNA remaining in A-conformation upon protein interaction.

3.8. Stability of protein–DNA and protein–RNA adducts

The protein–DNA and protein–tRNA binding constants estimated by UV-visible spectroscopy are presented in Table 2. The UV absorption spectra of protein–polynucleotide complexes are calculated using the double reciprocal plot of $1/(A - A_0)$ vs. $1/$(protein concentration), which is linear and the binding constant (K) can be estimated from the ratio of the intercept to the slope. A_0 is the initial absorbance of the free DNA or RNA at 260 nm and A is the recorded absorbance of polynucleotides in the presence of different protein concentrations. The overall binding constants for protein–DNA and protein–RNA complexes are given in Table 2). HSA–DNA complexes showed two bindings with $K_1 = 4.5 \times 10^5$ M^{-1} and $K_2 = 6.1 \times 10^4$ M^{-1}, while one binding with $K = 1.45 \times 10^4$ M^{-1} was observed for HSA–tRNA adducts (Table 2). Similarly, one binding was observed for RNase–DNA with $K = 6.1 \times 10^4$ M^{-1}, RNase–tRNA with $K = 4.0 \times 10^5$ M^{-1}, DNase–DNA with $K = 5.7 \times 10^5$ M^{-1} and DNase–tRNA with $K = 2.1 \times 10^4$ M^{-1} (Table 2). The stability of the protein–nucleic acids complexes are consistent with the binding constants of other protein–DNA and protein–RNA complexes [68–71]. It is worth mentioning that there has been no digestion of DNA by DNase I or tRNA by RNase A because no major structural changes occurred for DNA or RNA under these experimental conditions (Figs 5, 6, 8, 9).

3.9. Summary and future directions

Structural analysis of protein–DNA and protein–RNA complexes are important for better understanding of molecular interactions that govern transcriptional regulation. Even though the driving forces moving protein into the major and minor grooves of DNA duplex are reviewed [72], each protein binding to DNA grooves induces specific structural alterations of DNA conformation. HSA binding occurred with major and minor groove of DNA and RNA duplexes as well as with the backbone PO_2 group. RNase A interactions with G–C bases and the PO_2 were predominant, while no DNA and RNA digestion occurred at our experimental condition. Similarly, DNase I bindings were mainly with the backbone phosphate group and the A–T bases in the minor groove of DNA and RNA duplexes with no polynucleotide hydrolysis. Protein–polynucleotide interaction altered protein secondary structure for RNase A and DNase I and induced a partial B to A–DNA transition, while RNA remained in A-conformation. Even though

Table 2
Binding constants for protein–DNA and protein–RNA complexes

DNA	Binding constant (M^{-1})
HSA	4.5×10^5 and 6.1×10^4
RNase A	6.1×10^4
DNase I	5.7×10^5
RNA	Binding constant (M^{-1})
HSA	1.45×10^4
RNase A	4.0×10^5
DNase I	2.1×10^4

FTIR spectroscopy proved to be a useful tool in determining the protein binding sites in the major or minor groove of nucleic acid duplexes and the structural variations of protein and DNA and RNA complexes, further study is needed to apply molecular modeling based on energy minimization to present proper structural models for protein–DNA and protein–RNA interactions.

Acknowledgements

This work is supported by grants from Natural Sciences and Engineering Research Council of Canada (NSERC) and FCAR (Québec).

References

[1] S.C. Harrison, A structural taxonomy of DNA-binding domains, *Nature* **353** (1991), 715–719.
[2] B.F. Luisi, DNA–protein interaction at high resolution, in: *DNA–Protein Structural Interactions*, D.M.J. Lilley, ed., Oxford University Press, New York, NY, 1995, pp. 1–48.
[3] N.M. Luscombe, S.E. Austin, H.M. Berman and J.M. Thornton, An overview of the structures of protein–DNA complexes, *Genome Biol.* **1** (2000), 1–37.
[4] N.M. Luscombe, A. Laskowski and J.M. Thornton, Amino acid-base interactions: a three-dimensional analysis of protein–DNA interactions at an atomic level, *Nucl. Acids Res.* **29** (2001), 2860–2874.
[5] M. Yonezawa, N. Doi, Y. Kawahashi, T. Higashinakagawa and H. Yanagawa, DNA display for *in vitro* selection of diverse peptide libraries, *Nucl. Acids Res.* **31** (2003), 1–5.
[6] I.V. Smolina, V.V. Demidov and M.D. Frank-Kamenetskii, Paulsing of DNA polymerases on duplex DNA templates due to ligand binding *in vitro*, *J. Mol. Biol.* **326** (2003), 1113–1125.
[7] T. Namanbhoy, A.J. Morales, A.T. Abraham, C.S. Vortler, R. Giege and P. Schimmel, Simultaneous binding of two proteins to opposite sides of a single transfer RNA, *Nature Struct. Biol.* **8** (2001), 344–348.
[8] D. Moras, Aminoacyl–tRNA synthetase, *Curr. Opin. Struct. Biol.* **2** (1998), 138–142.
[9] G. Varani and K. Nagai, RNA recongnition by NPR protein during RNA processing, *Annu. Rev. Biophys. Biomol. Struct.* **27** (1998), 407–445.
[10] S. Jones, D.T.A. Daley, N.M. Luscombe, H.M. Berman and J.T. Thornton, Protein–RNA interactions: a structural analysis, *Nucl. Acids Res.* **29** (2001), 943–954.
[11] G.C. Foulds and H. Etzkom, A capillary electrophoresis mobility shift assay for protein–DNA binding affinities free in solution, *Nucl. Acids Res.* **26** (1998), 4304–4305.
[12] C. Li and L.M. Martin, A robust method for determining DNA binding constants using capillary zone electrophoresis, *Anal. Biochem.* **263** (1998), 72–78.
[13] J. Xian, M.G. Harrington and E.H. Davidson, DNA–protein binding assays from a single sea urchin egg: A high-sensitive capillary electrophoresis method, *Proc. Natl. Acad. Sci. USA* **93** (1996), 86–90.
[14] T. Guszcynski and T.D. Copeland, A binding shift assay for the zinc-bound and zinc-free HIV-1 nucleocapsid protein by capillary electrophoresis, *Anal. Biochem.* **260** (1998), 212–217.
[15] T. Peters, *All about Albumin. Biochemistry, Genetics and Medical Application*, Academic Press, San Diego, CA, 1996.
[16] D.C. Carter and J.X. Ho, Structure of serum albumin, *Adv. Protein Chem.* **45** (1994), 153–203.
[17] S. Sugio, A. Kashima, S. Mochizuki, M. Noda and K. Kobayashi, Crystal structure of human serum albumin at 2.5 Å resolution, *Protein Eng.* **12** (1999), 439–446.
[18] H.M. He and D.C. Carter, Atomic structure and chemistry of human serum albumin, *Nature* **358** (1992), 209–215.
[19] T. Peters, Serum albumin, *Adv. Protein Chem.* **37** (1985), 161–245.
[20] S. Curry, P. Brick and N.P. Frank, Fatty acid binding to human serum albumin: New insights from crystallographic studies, *Biochim. Biophys. Acta* **1441** (1999), 131–140.
[21] I. Petitpas, T. Grune, A.A. Battacharya and S. Curry, Crystal structure of human serum albumin complexed with monounsaturated and polyunsaturated fatty acids, *J. Mol. Biol.* **314** (2001), 955–960.
[22] L. Painter, M.M. Harding and P.J. Beeby, Synthesis and interaction with human serum albumin of the first 3,18-disubstituted derivative of bilirubin, *J. Chem. Soc., Perkin Trans.* **18** (1998), 3041–3044.
[23] J.F. Riordan, *Ribonucleases: Structure and Functions*, G. D'Alessio and J.F. Riordan, eds, Academic Press, New York, NY, 1997, pp. 445–489.
[24] R.T. Raines, Ribonuclease A, *Chem. Rev.* **98** (1999), 1045–1065.

[25] J.L. Neira, P. Sevilla, M.A. Margarita, B. Marta and R. Manuel, Hydrogen exchange in ribonuclease A and ribonuclease S: Evidence for residual structure in the unfolded state under native condition, *J. Mol. Biol.* **285** (1999), 627–643.
[26] J. Matousek, G. Gotte, P. Pouckova, J. Soucek, T. Slavik, F. Vottariello and M. Libonatti, Antitumor activity and other biological actions of oligomers of ribonuclease A, *J. Biol. Chem.* **278** (2003), 23817–23822.
[27] R. Berisio, F. Sica, V.S. Lamzin, K.S. Wilson, A. Zagari and L. Mazzarella, Atomic resolution structures of ribonuclease A at six pH values, *Acta Crystallogr.* **D58** (2002), 441–450.
[28] P. Fu, J. Chen, Y. Tian, T. Watkins, X. Cui and B. Zhao, Anti-tumor effect of hematopoietic cells carrying the gene of ribonuclease inhibitor, *Cancer Gene Ther.* **12** (2005), 268–275.
[29] M.C. Haigis, E.L. Kurten, R.L. Abel and R.T. Raines, KFERQ sequence in ribonuclease A-mediated cytotoxicity, *J. Biol. Chem.* **277** (2002), 11576–11582.
[30] K.A. Dickson, C.L. Dahlberg and T.R. Raines, Compensating effects of the cytotoxicity of ribonuclease A variants, *Arch. Biochem. Biophys.* **415** (2003), 172–177.
[31] P.A. Leland, L.W. Schultz, B.M. Kim and R.T. Raines, Ribonuclease A variants with potent cytotoxic activity, *Proc. Natl. Acad. Sci. USA* **95** (1998), 10407–10412.
[32] T. Soucek, R.T. Raines, M. Haugg, S.A. Raillard-Yonn and S.A. Benner, Structural changes of ribonuclease A and their effects on biological activity, *Comp. Biochem. Physiol. Part C* **123** (1999), 103–111.
[33] C.G. Dos Remedios, D. Chhabra, M. Kekic, I.V. Dedova, M. Tsubakihara, D.A. Berry and N.J. Nosworthy, Actin binding proteins: Regulation of cytoskeletal microfilaments, *Physiol. Rev.* **83** (2003), 433–473.
[34] V.W. Campbell and D.A. Jackson, The effect of divalent cations on the mode of action of DNase I, *J. Biol. Chem.* **255** (1980), 3726–3735.
[35] P.A. Price, Characterization of Ca^{2+} and Mg^{2+} binding to bovine pancreatic deoxyribonuclease, *J. Biol. Chem.* **247** (1972), 2895–2899.
[36] S. Cal, K.L. Tan, A. McGregor and B.A. Connolly, Conversion of bovin pancreatic DNase I to repair endonuclease with a high selectivity for abasic sites, *EMBO J.* **17** (1998), 7128–7138.
[37] C.Q. Pan and R.A. Lazarus, Hyperactivity of human DNase I variants, *J. Biol. Chem.* **273** (1998), 11701–11708.
[38] A. Lahm and D. Suck, DNase I-induced DNA conformation: 2 Å structure of a DNase I–octamer complex, *J. Mol. Biol.* **221** (1991), 645–667.
[39] S.A. Weston, A. Lahm and D. Suck, X-ray structure of the DNase I–d(GGTATACC)$_2$ complex at 2.3 Å resolution, *J. Mol. Biol.* **226** (1992), 1237–1256.
[40] M.E. Reichmann, S.A. Rice, C.A. Thomas and P. Doty, A further examination of the molecular weight and size of deoxypentose nucleic acid, *J. Am. Chem. Soc.* **76** (1954), 3047–3053.
[41] R. Vijayalakshmi, M. Kanthimathi and V. Subramanian, DNA cleavage by a chromium(III) complex, *Res. Commun.* **271** (2000), 731–734.
[42] S. Alex and P. Dupuis, FTIR and Raman investigation of cadmium binding by DNA, *Inorg. Chim. Acta* **157** (1986), 271–281.
[43] A.A. Ouameur and H.A. Tajmir-Riahi, Structural analysis of DNA interactions with biogenic polyamines and cobalt(III)hexamine studied by Fourier transform infrared and capillary electrophoresis, *J. Biol. Chem.* **279** (2004), 42041–42053.
[44] D.M. Byler and H. Susi, Examination of the secondary structure of protein by deconvoluted FTIR spectra, *Biopolymers* **25** (1986), 469–487.
[45] W.C. Johnson, Analyzing protein circular dichroism spectra for accurate secondary structure, *Protein Struct. Funct. Genet.* **35** (1999), 307–312.
[46] N. Sreerama and R.W. Woddy, Estimation of protein secondary structure from circular dichroism spectra: Comparison of CONTIN, SELCON and CDSSTR methods with an expanded reference set, *Anal. Biochem.* **287** (2000), 252–260.
[47] J.J. Stephanos, Drug–protein interactions. Two-site binding of heterocyclic ligands to a monomeric haemoglobin, *J. Inorg. Biochem.* **62** (1996), 155–169.
[48] J.J. Stephanos, S.A. Farina and A.W. Addison, Iron ligand recognition by monomeric hemoglobins, *Biochim. Biophys. Acta* **1295** (1996), 209–221.
[49] M. Loprete and K.A. Hartman, Conditions for the stability of the B, C and Z structural forms of poly(dG-dC) in the presence of lithium, potassium, magnesium, calcium and zinc cations, *Biochemistry* **32** (1993), 4077–4082.
[50] E. Taillandier and J. Liquier, Infrared spectroscopy of DNA, *Methods Enzymol.* **211** (1992), 307–335.
[51] E.B. Starikov, M.A. Semenov, V.Y. Maleeve and A.I. Gasan, Evidential study of correlated events in biochemistry: physicochemical mechanisms of nucleic acid hydration as revealed by factor analysis, *Biopolymers* **31** (1991), 255–273.
[52] R. Ahmad, H. Arakawa and H.A. Tajmir-Riahi, A comparative study of DNA binding to Mg(II) and Ca(II) in aqueous solution: Major and minor grooves bindings, *Biophys. J.* **84** (2003) 2460–2466.
[53] S.B. Dev and L. Walters, Fourier transform infrared spectroscopy of the characterization of a model peptide–DNA interaction, *Biopolymers* **29** (1990), 289–299.

[54] A. Podesta, M. Indrieri, D. Brogioli, G.S. Manning, P. Milani, R. Guerra, L. Finzi and D. Dunlap, Positively charged surfaces increase the flexibility of DNA, *Biophys. J.* **89** (2005), 2558–2563.
[55] S. Krimm and J. Bandekar, Vibrational spectroscopy and conformation of peptides, polypeptides, and proteins, *Adv. Protein Chem.* **38** (1986), 181–364.
[56] A.A. Ouameur, E. Mangier, R. Rouillon, R. Carpentier and H.A. Tajmir Riahi, Effects of organic and inorganic polyamine cations on the structure of human serum albumin, *Biopolymers* **73** (2004), 503–509.
[57] S. Seshardi, K.A. Oberg and A.L. Fink, Thermally denatured ribonuclease A retains secondary structure as shown by FTIR, *Biochemistry* **33** (1994), 1351–1355.
[58] J.C. Fontecilla-Camps, R. de Llorens, M.H. le Du and C.M. Cuchillo, Crystal structure of ribonuclease A: d(ApTpApApG) complex, *J. Biol. Chem.* **269** (1994), 21526–21531.
[59] W. Kabsch, H.G. Mannherz, D. Suck, E.F. Pai and K.C. Holmes, Atomic structure of the actin: DNase I complex, *Nature* **347** (1990), 37–44.
[60] H.A. Tajmir-Riahi, J.F. Neault and M. Naoui, Does DNA acid fixation produce left-handed Z structure?, *FEBS Lett.* **370** (1995), 105–108.
[61] H. Malonga, H. Arakawa, J.F. Neault and H.A. Tajmir-Riahi, DNA interaction with human serum albumin studied by affinity capillary electrophoresis and FTIR spectroscopy, *DNA Cell Biol.* **25** (2006), 63–68.
[62] H. Malonga, H. Arakawa, J.F. Neault and H.A. Tajmir-Riahi, Transfer RNA binding to human serum albumin: A model for protein–RNA interaction, *DNA Cell Biol.* **25** (2006), 393–398.
[63] M. Vorlickova, Conformational transitions of alternating purin–pyrimidin DNAs in perchlorate ethanol solutions, *Biophys. J.* **69** (1995), 2033–2043.
[64] J. Kypr and M. Vorlickova, Circular dichroism spectroscopy reveals invariant conformation of guanine runs in DNA, *Biopolymers* **67** (2002), 275–277.
[65] B.I. Kankia, V. Bukin and V.A. Bloomfiled, Hexamine cobalt(III)-induced condensation of calf-thymus DNA: circular dichroism and hydration measurements, *Nucl. Acids Res.* **29** (2001), 2795–2801.
[66] C.N. N'soukpoé-Kossi, C. Ragi and H.A. Tajmir-Riahi, DNA interaction with RNase A alters protein conformation, *DNA Cell Biol.* **26** (2007), 28–35.
[67] C.N. N'soukpoé-Kossi, C. Ragi and H.A. Tajmir-Riahi, RNase A–tRNA binding alters protein conformation, *Biochem. Cell Biol.* **85** (2007), 311–318.
[68] S.J. Koch, A. Shundrovsky, B.J.C. Jantzen and M.D. Wang, Probing protein–DNA interactions by unzipping of a single DNA double helix, *Biophys. J.* **83** (2002), 1098–1105.
[69] G. Wieland, P. Hemerich, M. Koch, T. Stoyan, J. Hegemann and S. Diekmann, Determination of the binding constants of the centromere protein Cbf1 to all 16 centeromer DNAs of *Saccharomyces cereviase*, *Nucl. Acids Res.* **29** (2001), 1054–1060.
[70] M. Lutsky and L.A. Mimy, Kinetics of protein–DNA interaction: Facilitated target location in sequence-dependent potential, *Biophys. J.* **87** (2004), 4021–4035.
[71] X. Xheng and C. Bevilacqua, Straightening of bulged RNA by double-stranded RNA-binding domain from the protein kinase PKR, *Proc. Natl. Acad. Sci. USA* **97** (2000), 14162–14167.
[72] P.L. Privalov, A.I. Dragan, C. Crane-Robinson, K.J. Brreslauer, D.P. Remeta and C.A.S.A. Minetti, What derives proteins into the major or minor grooves of DNA?, *J. Mol. Biol.* **365** (2007), 1–9.

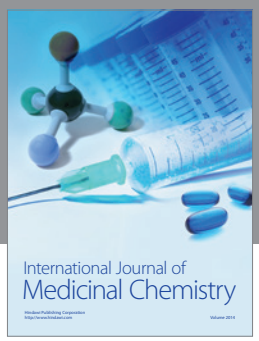

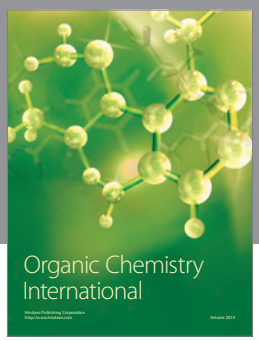

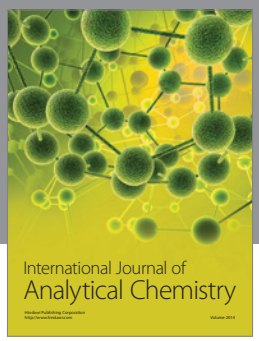

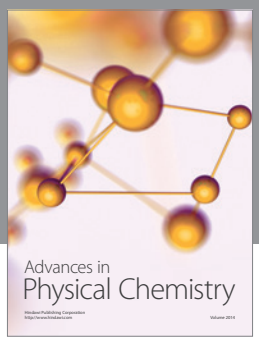

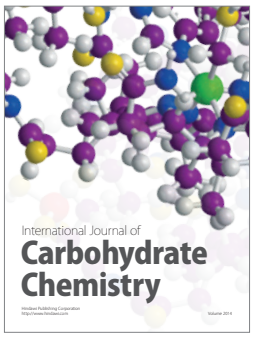

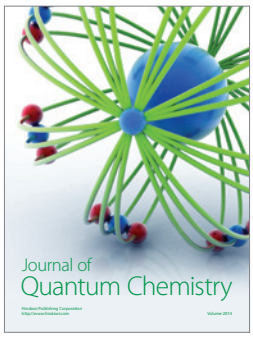

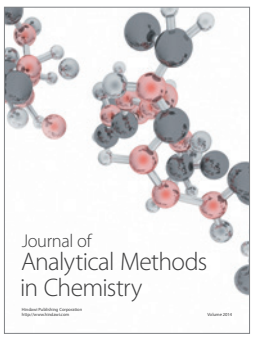

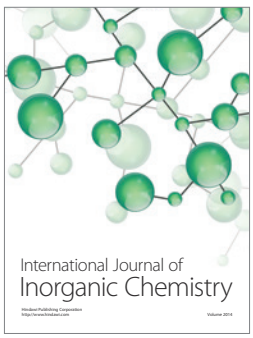

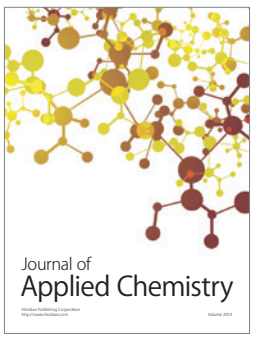

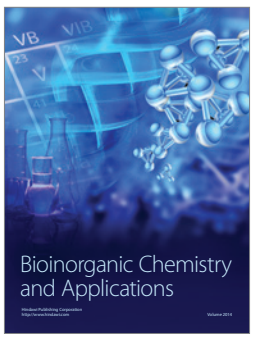

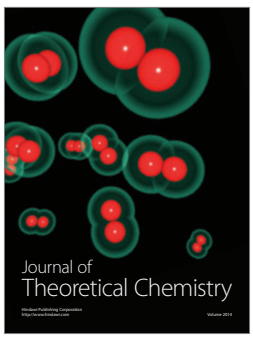

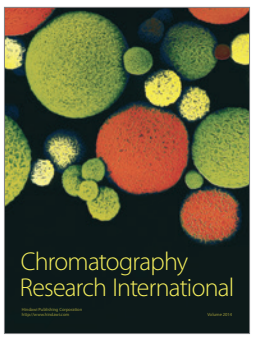

Hindawi

Submit your manuscripts at
http://www.hindawi.com